The persistence of regular reflection during strong shock diffraction over rigid ramps

By L. F. HENDERSON[1]†, K. TAKAYAMA[1],
W. Y. CRUTCHFIELD[2] AND S. ITABASHI[1]

[1]Shock Wave Research Center, Institute of Fluid Science, Tohoku University, Katahira, Aoba, Sendai 980-8577, Japan

[2]Center for Computational Sciences and Engineering, Lawrence Berkeley National Laboratory, Berkeley, CA 94720, USA

We report on calculations and experiments with strong shocks diffracting over rigid ramps in argon. The numerical results were obtained by integrating the conservation equations that included the Navier–Stokes equations. The results predict that if the ramp angle θ is less than the angle θ_e that corresponds to the detachment of a shock, $\theta < \theta_e$, then the onset of Mach reflection (MR) will be delayed by the initial appearance of a precursor regular reflection (PRR). The PRR is subsequently swept away by an overtaking corner signal (*cs*) that forces the eruption of the MR which then rapidly evolves into a self-similar state. An objective was to make an experimental test of the predictions. These were confirmed by twice photographing the diffracting shock as it travelled along the ramp. We could get a PRR with the first exposure and an MR with the second. According to the von Neumann perfect gas theory, a PRR does not exist when $\theta < \theta_e$. A viscous length scale x_{int} is a measure of the position on the ramp where the dynamic transition PRR $\to$ MR takes place. It is significantly larger in the experiments than in the calculations. This is attributed to the fact that fluctuations from turbulence and surface roughness were not modelled in the calculations. It was found that $x_{int} \to \infty$ as $\theta \to \theta_e$. Experiments were done to find out how x_{int} depended on the initial shock tube pressure p_0. The dependence was strong but could be greatly reduced by forming a Reynolds number based on x_{int}. Finally by definition, regular reflection (RR) never interacts with a boundary layer, while PRR *always* interacts; so they are different phenomena.

1. Introduction

Von Neumann (1943) studied the theory of reflecting shock waves. He solved the problems of regular reflection (RR) and *strong* Mach reflection (MR) completely for the special case of a perfect gas equation of state. As is well known (Hornung, Oertel & Sandeman 1979; Hornung 1986) three criteria have been proposed to determine the transition RR $\rightleftharpoons$ MR between the two reflecting systems. These are the detachment (*e*), the sonic (*s*) and the mechanical equilibrium (*N*) criteria. They are illustrated in the shock polar (δ, P) plane in figure 1 (Courant & Friedrichs 1948), where in shock-fixed coordinates δ is the streamline deflection angle across the shock, and Δp is the pressure jump across it. For a perfect gas the occurrence of any of them will

† Permanent address: 8 Damour Avenue, East Lindfield, Sydney NSW 2070, Australia.
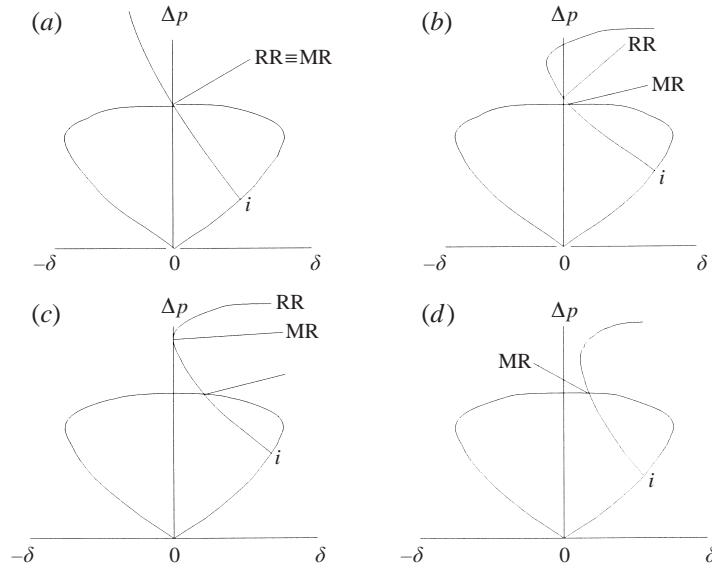
FIGURE 1. Shock polar diagrams for regular and Mach reflection in an ideal gas. (*a*) Mechanical equilibrium point θ_N; (*b*) arbitrary point in the bi-stable domain $\theta_e < \theta < \theta_N$; (*c*) detachment point θ_e; (*d*) $\theta < \theta_e$, where only the MR solution exists.

depend on a particular set of values of the shock system parameters (γ, M_i, θ), where γ, is the ratio of specific heats, M_i is the Mach number of the incident shock (*i*), and θ is the ramp angle (figure 2). Numerical values of θ_e, θ_s, and θ_N, corresponding to the system parameters of the present study are listed in table 1.

Experimenters have found the following three difficulties with the perfect gas theory.

The von Neumann paradox: For some parameter domains, there are no physically meaningful solutions to the MR theory, especially when the incident shock is weak. Yet experiments detect an irregular reflection that resembles an MR, for example Smith (1945), Bleakney & Taub (1949), Kawamura & Saito (1956), Henderson & Siegenthaler (1980), Lock & Dewey (1989), Sasoh, Takayama & Saito (1992), Sasoh & Takayama (1994), to mention only some of many papers. Recently, Colella & Henderson (1990) concluded that the irregular reflection was basically different from an MR, and named it a von Neumann reflection (VNR) see also Sasoh *et al.* (1992) and Henderson & Menikoff (1997, 1998).

The bi-stable domain: From the polar-plane analysis of shock reflection it is known that there is a restricted domain of parameters where RR and MR are both possible. For given (γ, M_i) the domain is defined by $\theta_e < \theta < \theta_N$ (figure 1*a–c*). Recent papers provide evidence that within this domain, the RR and MR systems are a bi-stable system. If this is correct then a fluctuation of suitable form and amplitude could force say an RR to change to an MR or vice versa. The bi-stability and or possibly related phenomena such as hysteresis have been studied by Chpoun *et al.* (1995), Vuillon, Zeitoun & Ben-Dor (1995), Ivanov *et al.* (1995*a,b*, 1996, 1997*a,b*), Fomin *et al.* (1996), Henderson, Crutchfield & Virgona (1997), Skews (1997), Henderson & Menikoff (1998).

The persistence of regular reflection: Another difficulty is that RR often appears in experiments when according to the perfect gas theory only MR should do so. Many of the references cited in the von Neumann paradox paragraph show signs
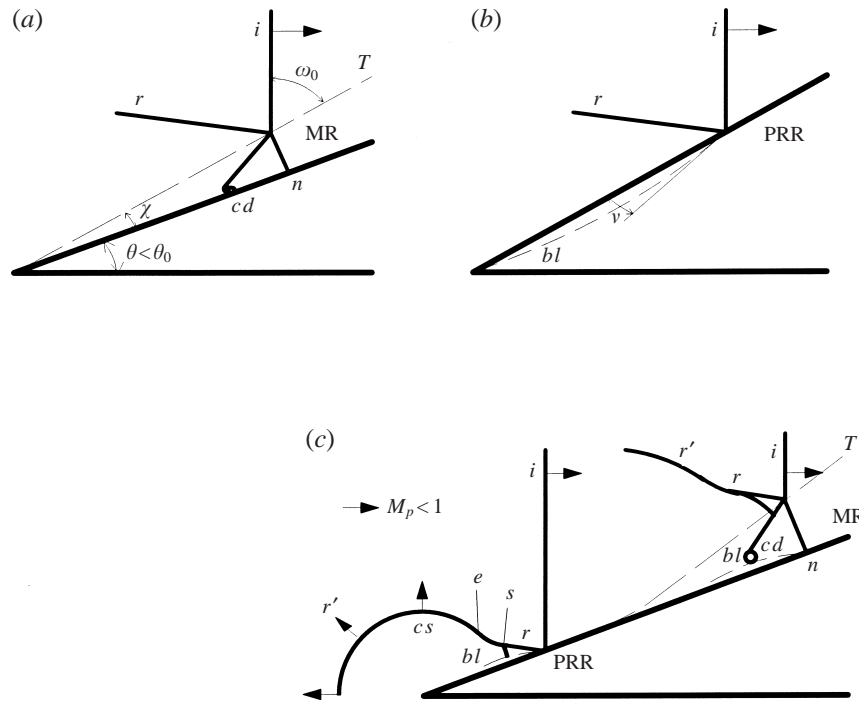
FIGURE 2. Shock diffractions predicted by Eular and Navier–Stokes calculations. (*a*) Euler, parallax assumption true; (*b*) N-S, parallax assumption, false; (*c*) negative boundary layer (*bl*) slope angle *v* in PRR node fixed coordinates. χ, Mach node trajectory angle; *T*, Mach node trajectory; *e, s*, detachment and sonic points on *r'* reflected shock, *cs*, corner signal.

θ_e (deg.)	θ_s (deg.)	θ_N (deg.)
53.776	53.924	57.021

TABLE 1. Shock reflection transition criteria when $\gamma = 5/3$, $M_i = 2.33$: θ_e, detachment; θ_s, sonic; θ_N, mechanical equilibrium.

of this phenomenon, but see also Henderson & Lozzi (1975), Henderson & Gray (1981), Hornung & Taylor (1982), Hornung (1986) and the low-density experiments of Walenta (1983, 1987). In the present paper the main concern will be this persistence. The bi-stable phenomenon will also be discussed but only so far as it influences the persistence of RR. The von Neumann paradox will not be considered.

In our earlier paper (Henderson *et al.* 1997, referred to as HCV97) we presented experimental data on strong shocks diffracting over rigid ramps. The experiments were done at the University of Sydney, and it is important to note that the scale of the experiments was about 0.040 m. This was the approximate distance that the incident shock *i* had travelled along the sloping surface of the ramp when its diffraction was photographed. Subsequently, the experiments were simulated numerically at the Lawrence Berkeley National Laboratory by integration of the conservation equations which included the Navier–Stokes (N-S) equations. It was clear from the data that a scale of 0.040 m was too small to make an adequate experimental test of the phenomena predicted by the calculations. The present authors decided to repeat the

Sydney experiments by using one of the larger shock tubes at the SWRC at Tohoku University. The ramp length scale was increased to 0.170 m.

Two sets of experimental data will be presented here. The first repeats the Sydney experiments on the larger scale, and it shows that 0.040 m was indeed too small. For example if the diffraction was photographed at 0.040 m one could observe a persistent regular reflection, but if it were photographed at 0.170 m one could observe a Mach reflection. Apart from the scale, the SWRC experiments were done for the same parameters as at Sydney. Specifically, rigid steel ramps were used with the same ramp angles θ, in argon gas with the same initial shock tube pressure $p_0 = 14.1$ kPa, at approximately the same room temperature $T_0 = 293.15 \pm 2$ K, and also with the same incident shock Mach number $M_i = 2.33 \pm 0.007$. In the second set of experiments the Reynolds number per metre (Re) was varied. If p_0 is the initial shock tube pressure then because $Re \propto p_0$, we could vary Re by a factor of about 7.6 by varying p_0 by the same factor. The results will show quite impressively the important effect that Re has on the phenomena.

The objectives of this paper are to make an experimental check on the predictions obtained from the calculations, and to explore the effects of the Reynolds number on the shock diffraction.

2. Formulation of the diffraction problem

2.1. *Constituitive relations*

Argon was chosen to simplify the physics. The dependence of the shear viscosity μ (hereafter the 'viscosity') on the temperature T, $\mu = \mu(T)$ was obtained by fitting an empirical relation to the viscosity tables in Hilsenrath *et al.* (1960), thus

$$\mu = \frac{2.01572 \times 10^{-6} T^{1.5}}{171.691 + T} \, \mathrm{kg\,m^{-1}s^{-1}}. \tag{2.1}$$

The tables were also used to obtain the specific heat at constant pressure C_p, the Prandtl number Pr, and the second virial coefficient of the equation of state (EOS). Since the virial term is small for the thermodynamic states of interest, it was sufficiently accurate to use the perfect gas EOS. Since both $Pr = 0.67$, and $C_p = 0.5203$ kJ kg^{-1} K^{-1}, can be taken as constants with negligible error, the thermal conductivity $k = k(T)$ was calculated from the definition of Pr,

$$k = \frac{C_p}{Pr}\mu, \tag{2.2}$$

so $k \propto \mu$. Therefore the flow dissipation can be characterized by a single parameter. It was convenient to choose the Reynolds number.

2.2. *The conservation equations*

These were the equations for the conservation of mass and energy, together with the Navier–Stokes (N-S) equations for two-dimensional, unsteady, compressible flow. They were presented in conservation form in HCV97. Occasionally it was of interest to compare the results obtained by replacing the N-S equations with the Euler equations, so both formulations were used.

2.3. *Ramp boundary conditions*

The ramp surface was assumed to be isothermal and always at room temperature, $T_0 = 293.15 \pm 2$ K. The error is negligible for this assumption (Mark 1958). Further-
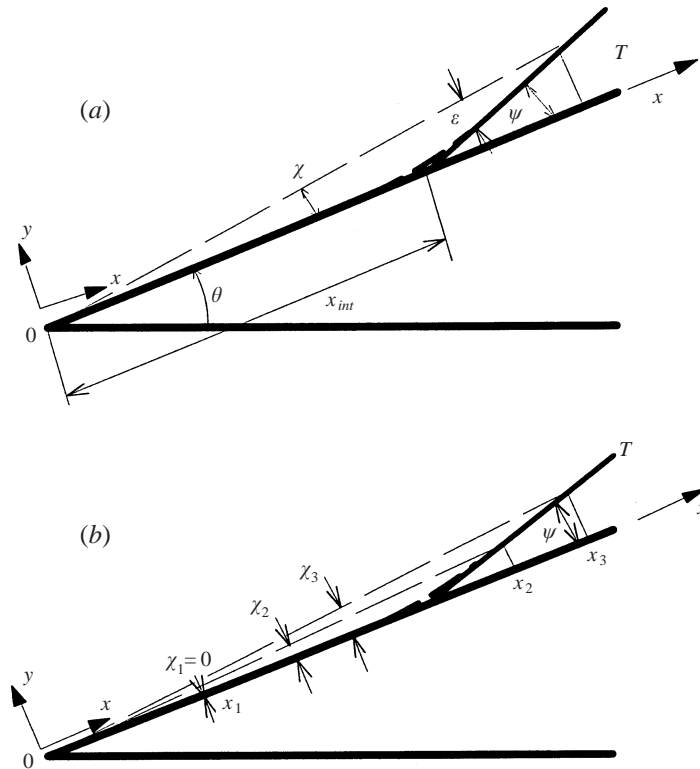
FIGURE 3. Illustration of how the trajectory angle χ depends on the x-coordinate, while the self-similar trajectory angle ψ does not depend on x when $x > x_{int}$. Note that $x_3 > x_2 > x_1 > 0$, implies that $\chi_3 > \chi_2 > \chi_1 = 0$, where $x_3 > x_2 > x_{int}$, and $x_1 < x_{int}$.

more the gas was assumed to be at rest on the ramp surface. We take the origin O of a rectangular coordinate system (x, y) to be at the ramp apex, x to be in the positive direction along the surface, y to be perpendicular to the surface, and (u, v) to be the corresponding components of the gas velocity (figure 3). The boundary conditions for the N-S formulation were thus

$$T_0 = 293.15\,\text{K}, \quad u = 0 = v. \tag{2.3}$$

These *isothermal-non-slip* conditions forced a laminar, heat-conducting boundary layer to be on the ramp surface. For the Euler formulation, the surface was adiabatic, with $v = 0$, and u unconstrained. They are *adiabatic-slip* boundary conditions.

3. The phenomena predicted by the calculations

3.1. *The Euler calculations*

These were done by Professor P. Colella of The University of California, Berkeley; his data were presented in HCV97. There was no boundary layer in this case. The von Neumann theory predicts that if $\theta < \theta_e$, a Mach reflection will appear at the instant the incident shock passes the apex. It also predicts that the MR will be self-similar, that is, it will grow uniformly with time. The Euler data support these predictions. In particular the trajectory of the shock triple point T (Mach node) was a straight line that passed through, or very close to, the ramp apex O. Experimentalists often assume

that the trajectory has this property; it is called the *parallax assumption* (HCV97). They measure the angle χ, which the trajectory makes with the ramp surface (figure 2*a*).

3.2. *The Navier–Stokes calculations for* $\theta < \theta_e$

3.2.1. *The precursor regular reflection*

The N-S results are very different from those from the Euler equation. It is predicted that initially there will be a precursor regular reflection (PRR), followed by a compressive disturbance, called 'the corner signal (*cs*)'. In time the *cs* overtakes the PRR and forces the eruption of the MR from the ramp surface (figure 2*c*). The PRR is therefore *unstable*, but because it exists for a time, we shall say instead that it is *meta-stable*. The trajectory *T* of the Mach node (shock triple point) is initially tangent to the ramp, but curves away from it and rapidly becomes a straight line. The growth of the MR becomes self-similar once the trajectory is straight. The N-S results also show that the MR is not self-similar but only asymptotically self-similar. Nevertheless, the detailed data demonstrate that an MR quickly becomes indistinguishable from a self-similar system. The development of self-similarity slows down as $\theta \to \theta_e$ from below.

The perfect gas (von Neumann) theory has no solutions for PRR when $\theta < \theta_e$. *The PRR solution provided by the N-S calculations depends on the presence of the boundary layer on the ramp.* If the origin of a rectangular Cartesian system (X, Y) is fixed with respect to the PRR node with X parallel to, and Y perpendicular to the ramp, then the boundary layer will have a negative displacement height in these coordinates (Mirels 1956; Mirels & Hamman 1962; Hornung *et al.* 1979; Hornung 1986). It also has a negative slope angle $v < 0$, say, at the PRR node which effectively relaxes the local boundary condition by this amount (figure 2*b*). The existence (and persistence) of the PRR when $\theta < \theta_e$ observed in experiments is caused by the boundary layer producing this relaxation. But for the perfect gas theory there is no boundary layer ($v = 0$) and no explanation for the PRR.

3.2.2. *The viscous length scale* x_{int}

If the straight part of the trajectory is projected onto the ramp surface it will intersect it at the point $x = x_{int}$ say; x_{int} will be defined to be the *viscous length scale* introduced into the flow by the boundary layer. It is a measure of the distance along the ramp where the dynamic transition PRR $\to$ MR takes place (figure 3*a*).

The N-S results show the importance of x_{int} for photographing ramp diffraction. If the photograph is taken when $x < x_{int}$ a PRR will be observed, but if taken when $x \gg x_{int}$, an MR will be observed. If it is taken when $x \approx x_{int}$ the diffracting system may not be optically resolvable.

3.2.3. *Dynamic transition*

In more detail, the N-S results predict that the corner signal (*cs*) has a sonic surface at its rear. The *cs* interacts with the reflected shock *r*, and forces it to bend smoothly into a steeper shock *r'*, say (figure 2*c*). The local wave angle of *r'* is steeper in places than the wave angles corresponding to both the shock sonic point *s*, and the detachment point *e*. As the *cs* overtakes the PRR node it smoothly sweeps away the *r* shock causing it to shrink and finally to disappear. The steeper *r'* shock then begins to overtake the node and first its sonic point *s*, and then its detachment point *e*, successively overtake. The Mach reflection erupts at or very near where the *e* point overtakes. The *r'* shock behaves like a bow shock detaching from a ramp whose angle θ is too steep to permit the shock to be attached to the apex. Thus the blockage

Argon; $M_i = 2.327 \pm 0.007$; $p_0 = 14.1\,\text{kPa}$; $T_0 = 293.15 \pm 2\,\text{K}$

| θ (deg.) | 34.6 | 38.6 | 44.0 | 50.5 | 52.0 |

TABLE 2. Parameter data for the 0.170 m scale shock tube experiments

caused by the ramp to the flow forces the detachment of r'. Additional support for this conclusion comes from the following fact. Because $M_i = 2.33$, the flow Mach number M_p of the argon is subsonic $M_p = 0.891 < 1$ along the shock tube in laboratory-frame coordinates. Therefore, the part of the r' shock that lies upstream of the ramp can never become attached to the apex; it must always propagate away from it.

Conclusion: The flow is determined by two disturbances: first by the blockage of the ramp which is dominant for the asymptotic flow; secondly by the boundary layer which initially suppresses the onset of Mach reflection over the length scale x_{int}. The criterion for the transition is at or close to the perfect gas (inviscid) detachment point e, which suggests that the process is dominated by the blockage, while the boundary layer dominates the distance (and time) delay of the transition.

3.3. *The Navier–Stokes calculations for $\theta \to \theta_e$, with $\theta < \theta_e$*

Here $\theta \to \theta_e$ from below. The cs slows down relative to the PRR node and has the same velocity as the node for θ a little less than θ_e; at say $\theta = \theta_{ob}$. From our earlier paper, a curve of best fit through the numerical data is

$$x_{int} = \frac{0.057243}{(53.6 - \theta)^2}, \tag{3.1a}$$

so $x_{int} \to \infty$ as $\theta \to \theta_{ob} = 53.6°$. At this condition the cs has the same velocity as the PRR node and the boundary layer stabilizers the PRR for all time. Referring to table 1, the hierarchy is $\theta_{ob} < \theta_e < \theta_s < \theta_N$, so $\theta_e = 53.776°$ is the closest of the perfect gas criteria to the numerical limit θ_{ob}.

Taking the square root of equation (3.1a), and then re-arranging, we get

$$\theta \sqrt{x_{int}} = -0.23926 + 53.6 \sqrt{x_{int}}. \tag{3.1b}$$

This will be more convenient because the right-hand side is now linear in $\sqrt{x_{int}}$.

4. The larger-scale experiments

4.1. *The shock tube*

The experiments were done in a $0.1778\,\text{m} \times 0.1016\,\text{m}$ shock tube with a 3 m long driver section, and a 15 m long driven section. It has a fast opening valve instead of a diaphragm which reduces the variation in M_i to $\pm 0.3\%$ for $1.5 \leqslant M_i \leqslant 5$. The shock speed was measured by seven Kistler pressure transducers (model 603B) spaced along the driven section. This section was evacuated to 0.1 kPa, and filled with argon to the required initial pressure p_0. Equilibrium for p_0 was established after about three minutes, and measured by a Tokyo Aircraft Instrument workshop test gauge, model 30021. It has 1000 graduations from 0 to $1.05\,\text{kg}\,\text{m}^{-2} \equiv 105\,\text{kPa}$.

As noted already, the parameters of the experiments were as closely as possible the same as those used in Sydney, except that the scale was 0.170 m instead of 0.040 m. The parameter data are given in table 2.
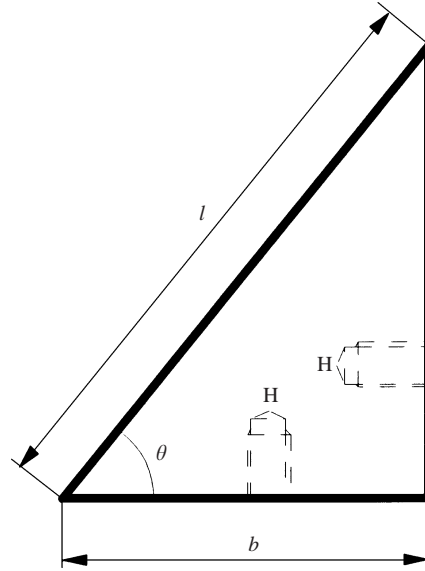
FIGURE 4. Design of the solid steel ramps. H, tapped holes for mounting in the shock tube.
See table 3 for dimensions.

θ (deg.)	34.6	38.6	44.0	50.5	52.0
b (mm)	96.33	106.6	117.88	131.34	134.08
l (mm)	170.01	170.36	169.77	170.16	170.17
R_a (μm)	0.165	0.093	0.120	0.492	0.168
R_{amax} (μm)	0.8	0.4	0.8	3.2	0.8
L (mm)	0.25	0.25	0.25	0.25	0.8

TABLE 3. Dimensions and surface roughnesses of the ramps shown in figure 4.

4.2. *The ramp design*

Five ramps were made of solid steel S45C; the design is shown in figure 4. The ramps spanned the shock tube, and the gaps at both ends were no more than 10 μm. The sloping surfaces of the ramps were specified to have a high quality commercial finish. Their dimensions and surface roughnesses (R_a), and maximum asperities (R_{amax}) are presented in table 3.

The surface roughness was measured over a distance L using a Kosaka Laboratory Ltd gauge, model SE-3AK. The average roughness R_a was found from

$$R_a = \frac{1}{L} \int_0^L |y| \, \mathrm{d}x. \tag{4.1}$$

When not in use the ramps were coated with grease to prevent corrosion. The grease was wiped off, and the surface swabbed with acetone before installing any ramp in the shock tube.

4.3. *The optical system*

This was a double exposure interferometer (Takayama 1983). The light source was a Lumonics HLS3 pulsed ruby laser. Its duration was about 30 ns, and the time
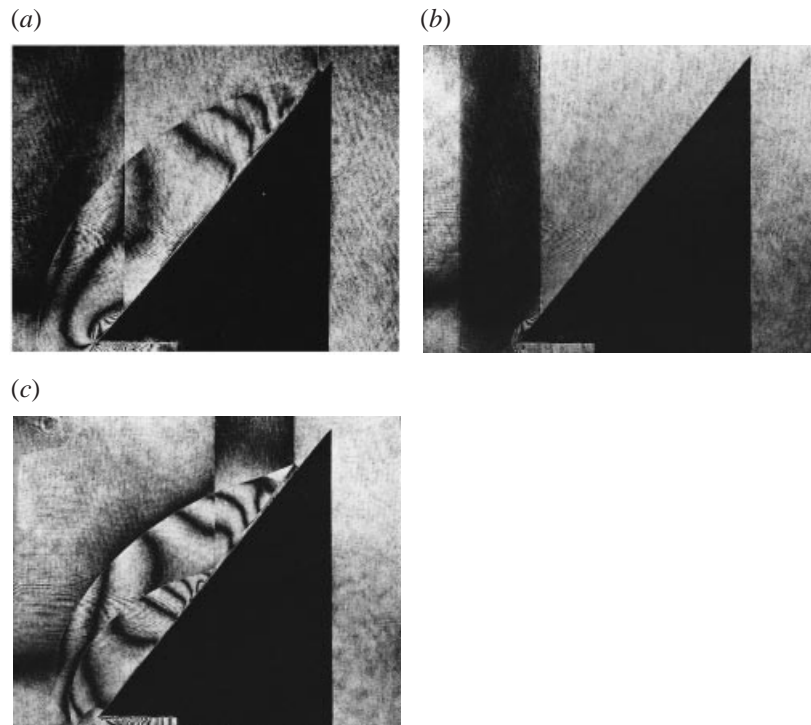
(*a*) (*b*)

(*c*)

FIGURE 5. Double exposure holographic interferograms of a diffracting shock propagating over a 52° ramp in argon gas, where $M_i = 2.33$, $p_0 = 14.1$ kPa. (*a*) Pre-cursor RR in early time exposure; MR in later time ($\Delta t = 120$ ms). (*b*) No diffraction in early time exposure, pre-cursor RR in later time ($\Delta t = 50$ ms); (*c*) MR in both early, and later time exposures ($\Delta t = 50$ ms).

interval between double pulses could be varied between 1 and 400 µs. The system was calibrated with a graticule and displayed negligible distortion. Consequently, there were no significant system errors in measuring the (x, y) coordinates of the Mach node trajectory.

4.4. *The experimental method*

The optical system was operated to record double exposures of the shock system as it travelled along a ramp. The double images were recorded on a holographic film. This technique enabled us to take, for example, an early time image to capture the predicted PRR, followed microseconds later by a second image to capture the predicted MR. The experiments were repeated 15 to 20 times, and at different time intervals, until enough data had been gathered to determine the Mach node trajectory accurately. A travelling microscope was used to scan the images, and to measure the (x, y) coordinates of the Mach node; the errors caused by the finite size of the node image were about ± 0.15 mm. The self-similar trajectory angle ψ, and the viscous length scale x_{int} were obtained from the (x, y) data.

5. Comparison of the Navier–Stokes results with experiment

5.1. *The existence of precursor regular reflection*

There are two exposures on the holographic film presented in figure 5(*a*). The first shows a PRR at $x = 0.0198$ m $< x_{int} = 0.0321$ m, while the second 120 µs later shows

θ (deg.)	34.6	38.6	44.0	50.5	52.0
ψ_{num} (deg.)	7.471	5.710	3.793	1.638	1.358
ψ_{exp} (deg.)	7.530	5.455	3.980	1.740	1.211
$x_{int\,num}$(m)	0.000368	0.000320	0.000814	0.005560	0.02760
$x_{int\,exp}$(m)	0.00282	0.00616	0.00560	0.0114	0.0321

TABLE 4. Comparison of the numerical with the experimental data for the self-similar trajectory angle ψ, and the dissipative length scale x_{int}.

an MR at $x = 0.1618$ m $> x_{int}$. The N-S results correctly predict a PRR followed by an erupting MR. For added clarity, the next holographic interferogram (figure 5b), captures the PRR by itself. This was done by taking the early time exposure before the incident shock had reached the ramp, and the later one such that, $0 < x < x_{int}$. In figures 5(a) and 5(b), the reflected shock (that is the union of r and r' shown in figure 2c) of the PRR appears to be curved everywhere. The x-coordinate of each of the PRR nodes was respectively 0.0198 m and 0.0181 m. By the N-S calculations the corner signal cs is less than 20 μm downstream of each node for these values of x. The numerical results also show that the reflected shock is only straight for the part, r, of the reflected shock that lies between the node and the cs. Our optical system cannot resolve 20 μm; for example the smallest length of a Mach shock that can be resolved is about 300 μm, although at this level the resolution may not be convincing. By contrast the N-S calculations can resolve about 2 μm, or two orders of magnitude better than the optics. So it is reasonable that the reflected shock should appear to be curved everywhere in figures 5(a) and 5(b). In figure 5(c), both of the exposures were for $x > x_{int}$, so the same MR appears at two different times, as also predicted by the N-S results.

Conclusion: Experiment confirms the prediction of the N-S calculations that a PRR exists by the action of the boundary layer, and that it exists only temporarily (meta-stability) before it is destroyed by eruption of the Mach reflection.

5.2. *The experimental data*

The experimental and numerical data for the (x, y) coordinates of the Mach node trajectory are presented in figure 6. The χ data for the 52° ramp are plotted in figure 7, and the (ψ, θ) data in figure 8. Evidently the numerical ψ data agree well with experiment, but the numerical x_{int} data show some discrepancy. A summary of the ψ, x_{int} data is presented in table 4.

5.3. *The parallax assumption and the $\chi(x)$ data*

This assumption was defined in HCV97.

Parallax assumption: When a plane shock diffracts over a rigid ramp with $\theta < \theta_e$, a self-similar Mach reflection is immediately obtained and its node trajectory is a straight line that passes through the ramp apex.

The calculated trajectories presented in HCV97 showed that the node was initially tangent to the ramp, then curved away from it and rapidly became a straight line. From this geometry it is apparent that the angle χ depends on *where* it is measured along the ramp, that is $\chi = \chi(x)$ (figure 3b). For example, $\chi = 0°$ when the PRR exists, but it grows monotonically from zero after the MR erupts. *So $\chi = \chi(x)$ is*
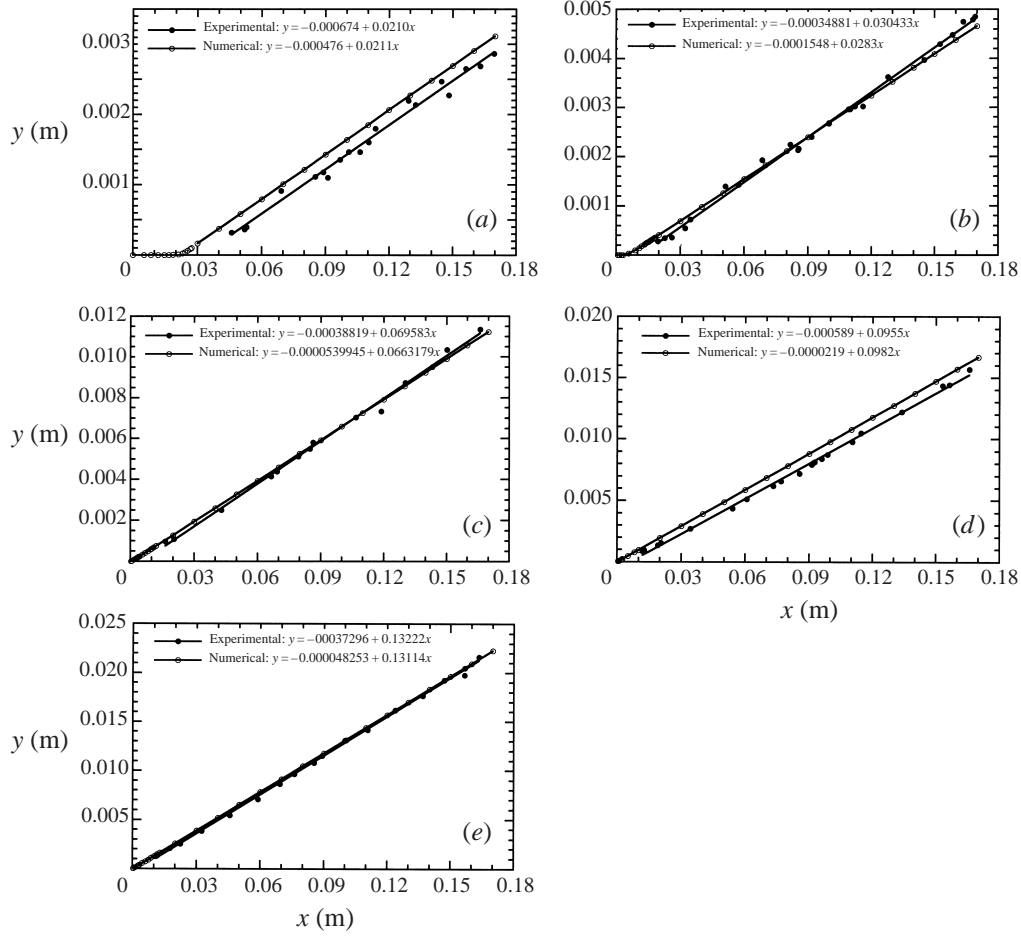
FIGURE 6. Comparison of the Navier–Stokes numerical data with experiment for the ramps listed in table 3. (*a*) $\theta = 52°$, (*b*) $\theta = 50.5°$, (*c*) $\theta = 44°$, (*d*) $\theta = 38.6°$, (*e*) $\theta = 34.6°$. Other parameters are, argon gas, $p_0 = 14.1\,\text{kPa}$; $T_0 = 293.15\,\text{K}$; $M_i = 2.33$.

not scale free. Thus the parallax assumption is wrong if a boundary layer is present. The appropriate trajectory angle to measure is the self-similar angle ψ, which is independent of any length or time scale (figure 3*a, b*). Clearly, the angle of parallax error for χ is

$$\epsilon = \psi - \chi. \tag{5.1}$$

Notice that asymptotically $\epsilon \to 0$ and $\chi \to \psi$.

The numerical and experimental data plotted in figure 7 confirm these results. Since $\chi = \tan^{-1} y/x$, and since also x_{int} is larger for experiment (table 4 and figure 6), then for a given $x > x_{int}$ the numerical y must be larger than the experimental y. Thus the numerical χ will also be the larger.

Conclusion: The N-S calculations correctly predict that the parallax assumption is wrong when a boundary layer is present.

Corollary: The trajectory angle χ of the Mach node depends on *where* it is measured along the ramp $\chi = \chi(x)$; it is not scale free and not a useful quantity to measure.
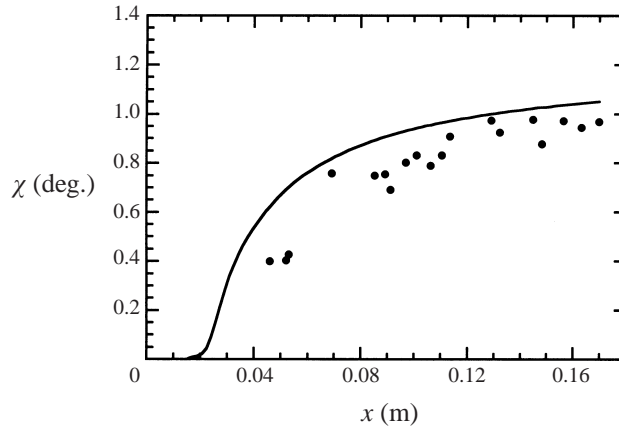
FIGURE 7. The Mach node trajectory angle χ versus x measured for the evolution of an MR on a 52° ramp in argon gas with $M_i = 2.33$, and $p_0 = 14.1$ kPa: ●, experimental data; curve is the N-S numerical data.

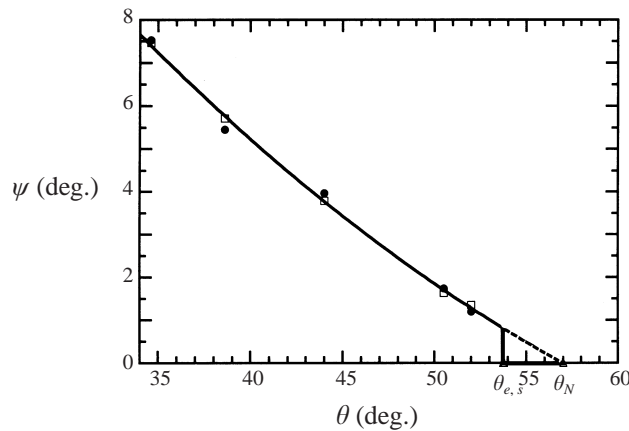FIGURE 8. Experimental and N-S data for the self-similar Mach node trajectory angle ψ versus the ramp angle θ, in argon gas with $M_i = 2.33$; $p_0 = 14.1$ kPa; $T_0 = 293.15$ K. ●, Experimental data; □, N-S data; curve is from equation (6.1), for the experimental data. Experimental error for ψ, ±0.1°; error negligible for θ.

5.4. *The self-similar trajectory angle ψ data*

The calculations in HCV97 showed that the Mach node trajectory asymptotes to a straight line, and that the approach to the asymptote slows down as $\theta \to \theta_e$ from below. If the calculations are terminated too soon the straight line slope would not be found with sufficient accuracy. Previously the termination was done subjectively, but for the numerical results reported here an objective method is used. The local slope for any x-coordinate can be estimated by differencing adjacent points on the trajectory. Since the shocks are resolved over two or three cells, the position of the node is always slightly ambiguous. Hence the data are noisy even though the calculation is free of noise. Values of the trajectory slope for the $\theta = 52°$ ramp as it approaches its asymptotic value ψ are shown in figure 9(*a*). The trajectory can be regarded as a straight line with negligible error when $x > 0.025$ m. The method was used to find the other numerical values of ψ versus θ presented in table 4 and figure
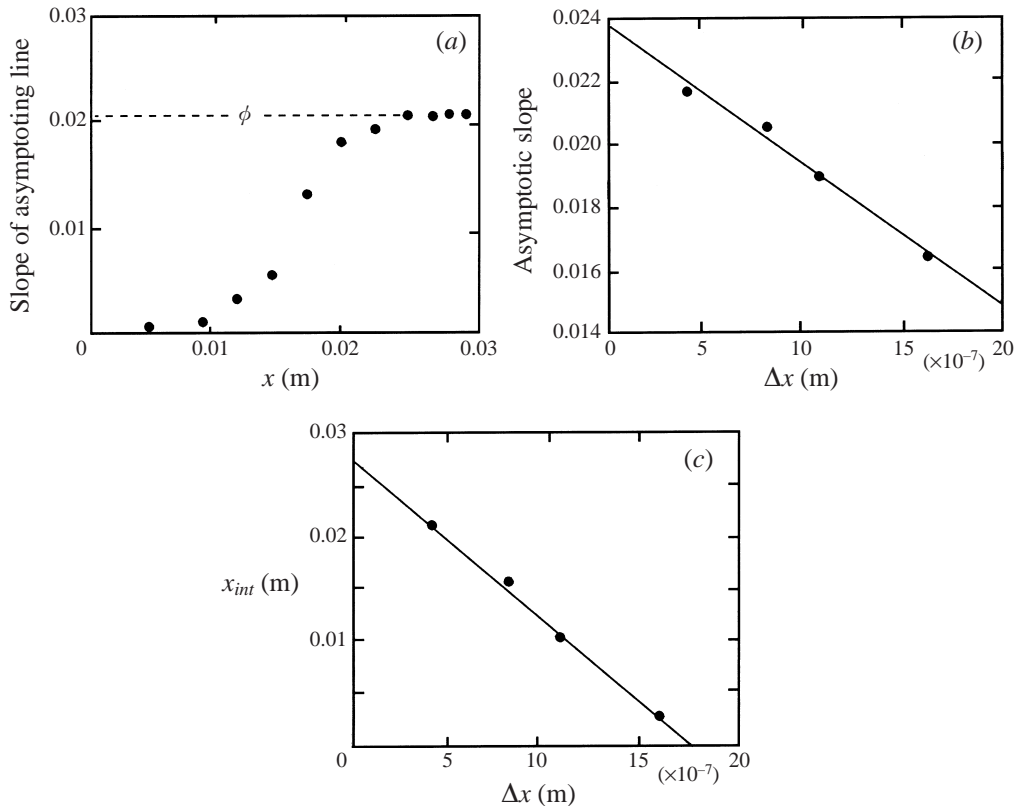
FIGURE 9. Study of the N-S numerical and asymptotic convergence for $\theta = 52°$, $M_i = 2.33$, $p_0 = 14.1\,\text{kPa}$, and $T_0 = 293.15\,\text{K}$ in argon gas. (*a*) Approximate slope of Mach node trajectory as a function of the distance x along the ramp, $\Delta x = 8.14 \times 10^{-7}\,\text{m}$; (*b*) slope of the asymptoting line as a function of Δx. The line is a least-squares linear fit to the data; (*c*) x_{int} as a function of Δx, the line is a least-squares linear fit to the data.

8; the experimental data for ψ are also presented and their error is about $\pm 0.1°$. The latter data are too noisy to support accurate slope differencing (figure 6). The differences between the numerical and the experimental data do not exceed $\pm 0.26°$, and there is no systematic discrepancy between them. The good agreement supports the conclusion that ψ is well enough determined to be independent of both x and the ramp length. For $p_0 = 14.1\,\text{kPa}$ the (x, y) data were measured over ramp lengths of $0.12\,\text{m}$ to $0.16\,\text{m}$. The ramp width is $0.1016\,\text{m}$ so the aspect ratio is in the range 0.63 to 0.83; thus three-dimensional effects could be significant. Each ramp forms a right-angled corner where it meets a shock tube wall, and there are shock/boundary-layer interactions in the corners. Now the calculations are two-dimensional, but because the numerical and experimental values of ψ are in good agreement, the experiments must also be nearly two-dimensional. Hence the ramp width $0.1016\,\text{m}$ is not a significant length scale for the ψ measurements, which means that three-dimensional effects are not significant either.

Conclusions: Slope differencing supports the conclusion that ψ can be accurately found when $x > 0.025\,\text{m}$, even for our least favourable case $\theta = 52°$. This is much less than the ramp lengths $0.17\,\text{m}$.

The two-dimensional calculations are in good agreement with experiment, which

implies that neither the ramp length nor its width are significant length scales in the measurements of ψ.

5.5. *The viscous length scale x_{int} data*

It is clear from the curve of best fit through the N-S data (3.1), that the $x_{int} \to \infty$ singularity is at $\theta = \theta_{ob} = 53.6° \approx \theta_e$. In our study it will be convenient to take the singularity to be at θ_e; it is certainly close to it. The linear form (3.1b) is compared with the experimental data in figure 10. The same discrepancy evident in table 4 and figure 6 is also evident there.

Using the same mathematical form, we found that a curve of best fit through the experimental data was

$$x_{int} = \frac{1}{(\theta_N - \theta)^2} \tag{5.2a}$$

or

$$\theta \sqrt{x_{int}} = -1 + \theta_N \sqrt{x_{int}},$$

where in the present case $\theta_N = 57.021°$ by table 1 and x_{int} is in m; therefore

$$\theta \sqrt{x_{int}} = -1 + 57.021 \sqrt{x_{int}}. \tag{5.2b}$$

Equation (5.2b) is plotted in figure 10 and it is a good fit to the experimental data. We now have the remarkable result that *the N-S data places the $x_{int} \to \infty$ singularity at θ_e, but the experimental data places it at θ_N.* There are two possible sources of the discrepancy, namely that our numerical method is deficient and or that our model of the physics is deficient.

5.6. *Refinements to the numerical method*

Assuming that the calculations in HCV97 were not sufficiently accurate, we sought to improve our methodology. Two methods were used. These were to monitor the slope changes of the trajectory by differencing, and to extrapolate the finite difference step Δx to zero. The slope difference refinement was discussed in §5.4; here we discuss the effect of the cell size refinement on ψ and x_{int}.

In HCV97 we showed that the trajectory changed if the resolution changed. Here we use an extrapolation technique to estimate the result if the calculations were fully resolved, that is if $\Delta x \to 0$. When the solution is smooth, there is a global error proportional to $(\Delta x)^2$, but when it is discontinuous (as with shocks), it is proportional to Δx. In HCV97, the empirical evidence indicated that the calculations were first-order convergent. Presumably, if they were done with Δx small enough to fully resolve the shocks and boundary layer, the convergence would be of second order. The thickness of the incident shocks in argon was about four mean free paths (m.f.p.). With the initial pressure $p_0 = 14.1\,\text{kPa}$ and with room temperature $T_0 = 293.15\,\text{K}$, m.f.p. $= 0.6\,\mu\text{m}$, so the shock thickness was about $2.4\,\mu\text{m}$. Since our finest resolution was $0.407\,\mu\text{m}$, the incident shock was close to being fully resolved on the finest grids. The boundary layer begins under the incident shock. If it can be assumed that its thickness is locally comparable to that of the shock, then it will also be close to full resolution at $2.4\,\mu\text{m}$. On this basis, the error in the calculations should be of first order down to about $2.4\,\mu\text{m}$, and in particular this should be true for the slopes ψ and the intercepts x_{int}. Therefore, it is expected that if several calculations differing only in resolution are compared, there will be a linear relation with Δx for ψ and x_{int}. Actually this was demonstrated down to our smallest cell size of $0.407\,\mu\text{m}$ for $\theta = 50.5°$ in HCV97. Figure 9(b) shows some asymptotic values of ψ for different

resolutions Δx when $\theta = 52°$. Also shown is the least-squares fit,

$$\psi \rightarrow 0.0237 - 4484\Delta x.$$

This straight line is an excellent fit to the data, as it should be if the numerical method is first-order convergent. If the convergence remains of first order down to $\Delta x = 0$, then the fully resolved value of $\psi = \tan^{-1} 0.237 = 1.358°$. Even if the convergence becomes of second order below $2.4\,\mu m$, ψ should remain close to the first-order value. The angle is also quite close to the value given by the Euler calculation where $\chi = \psi = 1.45°$. In figure 9(c), the same type of calculation finds x_{int}. The straight line of best fit is

$$x_{int} \rightarrow 0.0276 - 15293\Delta x,$$

so that $x_{int} = 0.0276\,m$, for the fully resolved calculation, while for experiment $x_{int} = 0.0321\,m$ (table 4). All the numerical data presented in table 4 have been refined in this way.

Conclusion: The discrepancy for x_{int} cannot be explained by insufficient resolution in the calculations.

5.7. *Deficiencies in the physical model*

Dimensionality: Figure 3 shows how x_{int} is obtained from ψ. Since the measurements of ψ are not significantly affected by the ramp dimensions (§ 5.4), this suggests that x_{int} is not affected either. We shall assume that this is correct. However, if the ramp width were modelled, it cannot be entirely ruled out that the numerical trajectories in figure 6 could be shifted somewhat to the right by three-dimensional effects.

Turbulence: The N-S equations can only model a laminar boundary layer. There are two sources of turbulence in the experiments. First, the incident shock produces a turbulent boundary layer as it travels along the driven section of the shock tube. Acoustic fluctuations radiate from it to every part of the flow downstream of the shock. Secondly the Reynolds number per metre just outside the boundary layer on the ramp is $Re \approx 10^7\,m^{-1}$, when $p_0 = 14.1\,kPa$. Therefore at $1\,cm$ behind the PRR node $Re \approx 10^5$, which implies that the boundary layer is turbulent. Turbulence increases the heat transfer coefficient (h) and this can be estimated empirically (Wong 1977, p. 73). Making h non-dimensional with the Nusselt number (hx/k), the ratio of the turbulent to laminar values of h is about $0.056Re^{0.3}$, or 1.8 when $Re \approx 10^5$. So it is plausible that turbulence contributes to the x_{int} discrepancy.

Ramp surface roughness: The average roughness varies within $0.093 \leqslant R_a \leqslant 0.492\,\mu m$, and the asperities within $0.4 \leqslant R_{amax} \leqslant 3.2\,\mu m$ (table 3). The smallest cell size used in the calculations was $0.407\,\mu m$, which is about the same as R_a but rather less than R_{amax}. If the initial boundary layer thickness is about the same as the incident shock ($2.4\,\mu m$), then R_a could be a significant length scale because it is of the same order. Roughness experiments have been done by Takayama & Ben-Dor (1981), and by Ben-Dor *et al.* (1987). Their smoothest surface had $R_a = 51.7\,\mu m$ which is two orders of magnitude larger than our R_a. The model size was the same as the Sydney experiments, $0.04\,m$. The gas was nitrogen and the values of p_0 were generally less than ours, although there was some overlap. Specifically, $0.00395 \leqslant p_0/p_a \leqslant 0.0658$, where p_a is the pressure of the standard atmosphere. They measured χ and not ψ. If p_0 and M_i were held constant, while the roughness was varied, the results showed that increasing roughness reduced the $\theta = \theta_{ob}$ where RR → MR was observed. This implies that x_{int} is increased by roughness and that R_a is a significant length scale. Thus roughness can in part account for the x_{int} discrepancy, but we did not model it.
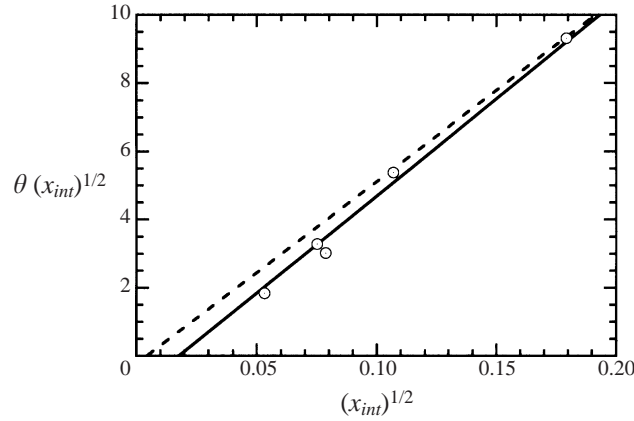
FIGURE 10. Comparison of the empirical formula for x_{int} versus θ with experiment. $\odot$, experimental data; full line from equation (5.2b), dashed line from equation (3.1b).
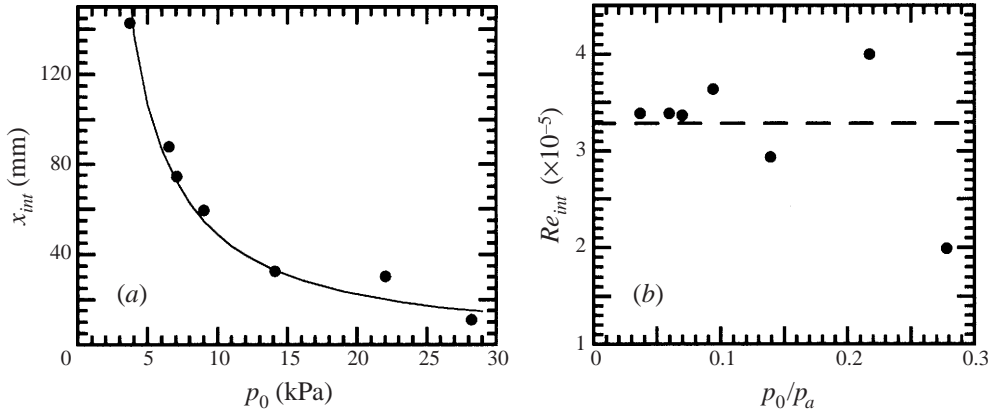

FIGURE 11. Experimental data for the effect of the initial pressure p_0 of the shock tube on the dissipative length scale x_{int}. (a) Dimensional data x_{int} (mm) versus p_0 (kPa). (b) Non-dimensional data Re_{int} versus p_0/p_a. ——, power law curve of best fit, equation (5.3); – – –, $\langle Re_{int} \rangle = 3.28 \times 10^{-5}$.

Hypothesis: The discrepancy between the calculated and experimental values of x_{int} is caused by the fluctuations from the flow turbulence and the surface roughness, neither of which were modelled in the calculations.

If the hypothesis is correct, x_{int} should depend on the Reynolds number per metre. Suppose that the system parameters (θ, M_i, T_0) are held constant, then the ratios T/T_0, p/p_0, ρ/ρ_0, μ/μ_0, are also constants; therefore for a perfect gas, $Re \propto \rho_0 \propto p_0$.

5.8. *The variable pressure p_0 experiments*

A series of experiments was done with the $\theta = 52°$ ramp with $M_i = 2.33 \pm 0.07$, and $T_0 = 293.15 \pm 2$ K held constant while p_0 was varied. The idea was to vary p_0 by a factor of 10, but engineering limitations of our shock tube limited it to about 7.6; specifically $3.7 \leqslant p_0 \leqslant 28.2$ kPa. The x_{int} and ψ versus p_0 data are presented in table 5. The (p_0, x_{int}) data are plotted in figure 11(a), and the (x, y) trajectory data for each p_0 are plotted in figure 12. A power law curve of best fit through the x_{int} data is

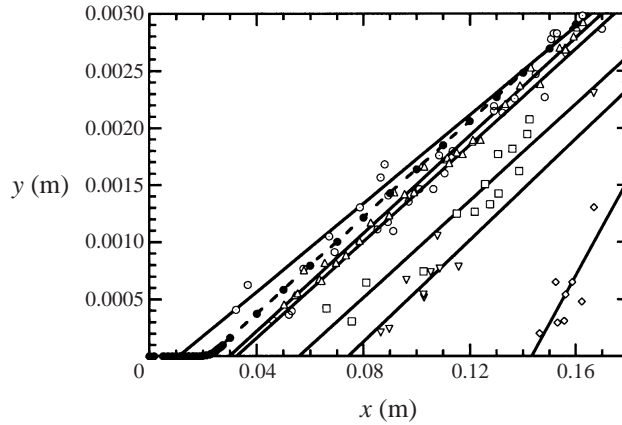$$x_{int}p_0^{9/8} = 650.185, \tag{5.3}$$

FIGURE 12. Experimental data on the effect of the initial pressure p_0 on the Mach node trajectory on the 52° ramp in argon gas with $M_i = 2.33$ and $T_0 = 293.15$ K; $\diamond$, $p_0 = 3.7$ kPa experiments; $\triangledown$, $p_0 = 7.05$ kPa; $\square$, $p_0 = 9.50$ kPa; $\bigcirc$, $p_0 = 14.1$ kPa; $\bullet$, N-S numerical data for $p_0 = 14.1$ kPa; $\triangle$, $p_0 = 22$ kPa; $\odot$, $p_0 = 28.2$ kPa. Full lines are linear curves of best fit.

p_0 (kPa)	3.7	6.00	7.05	9.5	14.1	22.0	28.2
p_0/p_a	0.0365	0.0592	0.0696	0.0938	0.139	0.217	0.278
x_{int} (mm)	143	88.1	74.6	59.7	32.5	30.4	11.0
$Re_{int} \times 10^{-5}$	3.60	3.59	3.58	3.58	3.11	4.54	2.11
ψ (deg.)	2.4	1.33	1.27	1.34	1.20	1.13	1.11

TABLE 5. Experimental data for the viscous length scale x_{int} and the self-similar trajectory angle ψ versus the initial shock tube pressure p_0.

where x_{int} is in mm and p_0 is in kPa. In SI units the constant is 1541.83. Note that x_{int} increases rapidly as p_0 decreases. Holograms for $p_0 = 3.7$ kPa are presented in figure 13. The increase of x_{int} for a smaller p_0 is clear if figure 13(*a*) is compared with figure 5(*a*) where $p_0 = 14.1$ kPa. Under the constraints on the experiments the kinematic viscosity should be inversely proportional to p_0, which suggests that $x_{int}p_0 =$ constant. But this not quite the same as for the experiment where the p_0 exponent is 9/8. However it does show that the rapid variation of x_{int} with p_0 can be greatly reduced by forming the Reynolds number

$$Re_{int} \equiv \frac{\rho V x_{int}}{\mu} \tag{5.4}$$

where V is the resultant flow velocity of a point just outside the boundary layer. If p_0 is also made non-dimensional then (5.3) becomes

$$Re_{int}(p_0/p_a)^{1/8} = 2.479 \times 10^5. \tag{5.5}$$

Hence Re_{int} varies only slowly with p_0/p_a when $\theta = 52°$. The non-dimensional curve of best fit is compared with experiment in figure 11(*b*). Note from figure 11(*a, b*) that the scatter in the data is enhanced by reducing the variation with p_0. This suggests that other, smaller effects are being revealed. They may be those discussed in § 5.7, but we do not have enough information to draw any conclusions. The self-similar trajectory angle ψ increases when p_0 decreases but the effect is small (table 5 and figure 12).
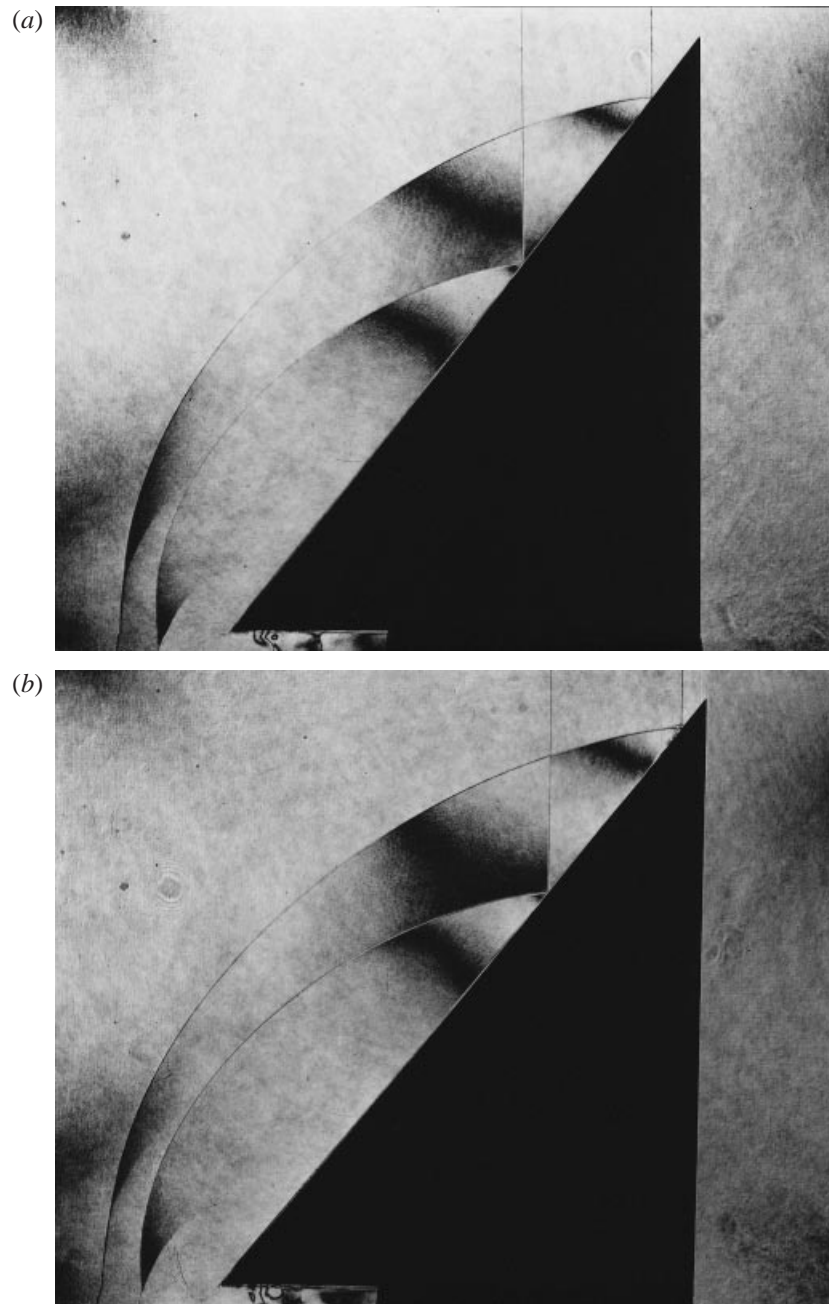
(a)

(b)

FIGURE 13. Double exposure holographic interferograms of a diffracting shock propagating over a 52° ramp in argon gas, where $M_i = 2.33$, $p_0 = 3.7\,\text{kPa}$. (a) PRR for both exposures; (b) PRR for the earlier exposure, and an MR for the later exposure.

This result is not surprising because ψ is an asymptotic quantity, so the boundary layer effect should be negligible. The larger change in ψ near the smallest $p_0 = 3.7\,\text{kPa}$ occurs because $x_{int} = 0.143\,\text{m}$ whereas the ramp length is $0.17\,\text{m}$ and there is only $0.027\,\text{m}$ available for measuring the trajectory. Thus the data are more scattered for this small length (figure 12) and the measurements of ψ and x_{int} are less accurate.
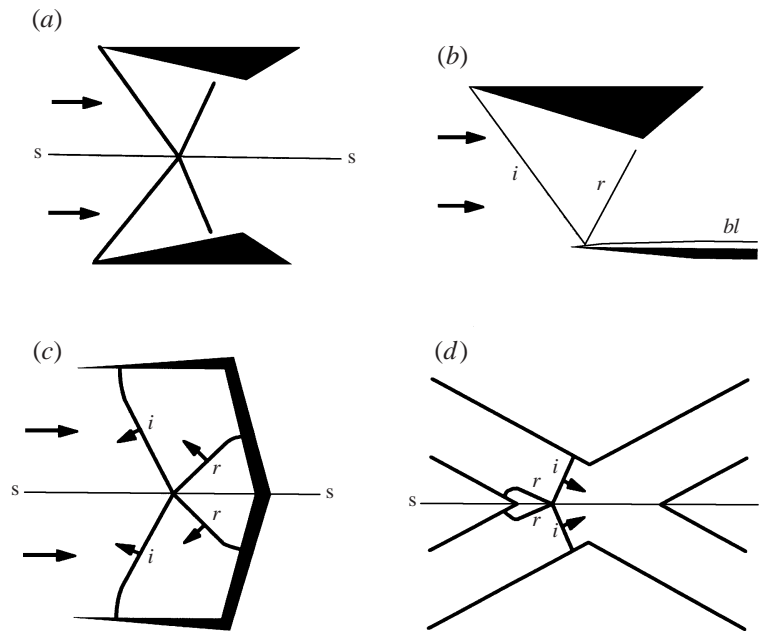
(a) (b)

(c) (d)

FIGURE 14. Model designs for generating self-similar and steady-state shock wave interactions: (a) supersonic wind tunnel model, steady state no *bl*; (b) supersonic wind tunnel model, steady state, short *bl*; (c) self-similar cavity design, no *bl*; (d) self-similar, bifurcated (crossed) shock tube design, no *bl*: *bl*, boundary layer; ss, plane of symmetry.

Conclusion: It is concluded that x_{int} varies rapidly with p_0 but only slowly with Re_{int}, while ψ varies only slightly with p_0.

6. The regular $\Longleftrightarrow$ Mach reflection transition criterion

6.1. *Steady-state transition with no boundary layer*

It is well known that two identical wedges can be arranged in a wind tunnel (or shock tunnel) so that their incident shocks meet on the plane of symmetry (figure 14a). The RR $\Leftrightarrow$ MR transition occurs without a boundary layer. It is convenient to discuss the reflections in terms of the angle α which the incident shocks make with respect to the on-coming flow. The angles $\alpha_e > \alpha_N$ correspond to the detachment and mechanical equilibrium criteria respectively. In earlier experiments α_N was found to be the criterion for the RR $\Leftrightarrow$ MR transition (Henderson & Lozzi 1975; Hornung & Kychakoff 1997; Hornung *et al.* 1979; Hornung & Robinson 1982).

Hysteresis: Hornung *et al.* (1979) predicted that the criterion for forward transition RR $\to$ MR, would be $\alpha_{tr}^F = \alpha_e$, but that for backward transition MR $\to$ RR, it would be $\alpha_{tr}^B = \alpha_N$. However Hornung & Robinson found that $\alpha_{tr}^F = \alpha_{tr}^B = \alpha_N$, that is, no hysteresis. Recently experiments by Chpoun *et al.* (1995) have found hysteresis, but unlike Hornung & Robinson they used an open jet tunnel, and their results were influenced by three-dimensional effects (Skews 1997; Ivanov *et al.* 1997b).

Ivanov *et al.* have made an extensive study of hysteresis. The results from their numerical simulations using Euler codes were that forward transition was close to α_e while the backward one was close to α_N. This was as predicted by Hornung *et al.* The experiments by Ivanov *et al.* in two different types of wind tunnels produced a more limited effect. In the tunnel with the larger acoustic fluctuations and with

Mach numbers (M) of 4 and 5, transition was within $1°$ of α_N when the aspect ratio ($g/w \equiv$ width/length) of the wedges was $g/w \geqslant 1$, but it differed from α_e by about $4.5°$. The hysteresis effect as measured by $\alpha_{tr}^F - \alpha_{tr}^B$ varied by only $0.03°$ to $0.29°$. But hysteresis was actually more pronounced than indicated by these small differences. For example, for RR $\rightarrow$ MR the MR appeared suddenly for a change in α of only $0.1°$ and the Mach shock length became 5% to 6% of the wedge length. The MR $\rightarrow$ RR transition was smoother. (Hornung *et al.* noticed the same effect.) Hysteresis was certainly found in the tunnel with the smaller acoustic fluctuations, and with $M = 6$. The difference $\alpha_{tr}^F - \alpha_{tr}^B$ varied between $2°$ and $3°$, compared to the numerical prediction of $\alpha_{tr}^F - \alpha_{tr}^B \equiv \alpha_e - \alpha_N = 10.51°$. Their experiments and Euler results support the conclusion that that both RR and MR are stable in the dual domain. Specifically their hypothesis was that in the dual domain, (*RR*) *is stable with respect to small perturbations but unstable to large perturbations. Moreover, the threshold amplitude decreases as* α *increases*. There are no free-stream perturbations in numerical simulations, which presumably allows regular reflection to exist up to α_e.

Henderson & Lozzi (1975) reflected a shock off a flat plate near its leading edge (figure 14*b*). The reflection occurred in the presence of a short boundary layer, and transition was close to α_N.

6.2. *Self-similar transition with no boundary layer*

Reflecting a plane shock from inside a symmetrical cavity (figure 14*c*) can produce self-similar reflections. The experimental results show that there is an MR in the dual domain and that α_N is the transition criterion (Henderson & Lozzi 1975; Virgona 1993). For the cavity design, there are acoustic fluctuations from the boundary layer on the walls of the driven section of the shock tube and the reflections propagate into this disturbed flow. Consequently there are perturbations upstream and downstream of the reflections. No RR or hysteresis has yet been reported in its dual domain. The design has a very limited domain of parameters. Skews has shown that it is practical to use a crossed shock tube design (figure 14*d*), and it should be more flexible (Barbosa, Skews & Felthun 1997). At the time of writing, no transition data are available from it.

In HCV97, we simulated self-similar reflection at a plane of symmetry with the N-S equations. In order to remove the boundary layer, we used the adiabatic-slip boundary conditions. The ramp surface could thus be considered to be equivalent to a plane of symmetry. Since there was no PRR the results for ψ versus θ were close to those of the Euler calculations for $\theta < \theta_e$. The computer cost was much less for these calculations and we were able to explore the θ_e point. We found that the curve had a discontinuity at θ_e. Specifically, there was an MR at $(\theta_e - 0.1)°$, and an RR at $(\theta_e + 0.1)°$. Thus the N-S calculations show that the MR $\rightarrow$ RR transition occurs at θ_e with these boundary conditions. (Note that for RR, θ_e and α_e are related by $\alpha_e = (90 - \theta_e)°$.) This result is contrary to the Euler calculations of Colella, and to the results of the cavity experiments, both of which place the transition at θ_N. This inconsistency was addressed in HCV97. Initially we set $\mu = 0 = k$, thereby reducing the N-S equations to Euler equations: an MR appeared, and after its Mach shock had grown to about $5\,\mu$m, μ and k were set to their correct values. The MR continued to grow. It was concluded that the MR was stable in the dual domain, but that it did not appear spontaneously because the fluctuations were not modelled. The Euler calculations of Ivanov *et al.* also placed the transition at α_N which is consistent with the results of Colella and experiment.

Conclusion: If in the dual domain self-similar reflection occurs without a boundary

layer, then cavity experiments and Euler calculations show that MR is stable, but N-S calculations show that RR is stable when there are no fluctuations. Thus for the stated conditions both RR and MR may be stable in the dual domain.

6.3. *Regular and persistent regular reflection*

We distinguish between regular and persistent regular reflection. The difference is that RR appears *without* a boundary layer, while PRR appears *with* a boundary layer.

Conclusion: Regular reflection occurs when a shock reflects off a plane of symmetry with $\alpha \leqslant \alpha_N$. It does not interact with any boundary layer and it is well described by the von Neumann theory.

PRR does interact with a boundary layer. It is clear that because the von Neumann theory ignores the boundary layer it cannot predict PRR. Thus RR and PRR are different phenomena. It is plausible that they would become identical if $Re \to \infty$. A PRR is meta-stable over the length x_{int} for all $\theta \leqslant \theta_e$, but it is stable for $\theta_e \leqslant \theta \leqslant \theta_N$ and for $\theta > \theta_N$ (§6.4). There is no PRR theory analogous to the von Neumann theory.

Conclusion: Persistent regular reflection occurs when a shock diffracts over ramp with $\theta < 90°$; it is meta-stable for $\theta < \theta_e$ and stable for $\theta \geqslant \theta_e$.

6.4. *Self-similar transition with a boundary layer*

The quadratic curve of best fit plotted through the (ψ, θ) data in figure 8 is

$$\psi = 27.1845 - 0.718948\theta + 0.004246671\theta^2 \tag{6.1}$$

where θ and ψ are in degrees, and $\theta < \theta_e$. Many experimenters have found that there is an 'RR' (or a PRR by our definition) when $\theta > \theta_e$ (Bleakney & Taub 1949; Kawamura & Saito 1956; Henderson & Lozzi 1975; Ben-Dor & Glass 1979, 1980). Henderson & Lozzi conjectured that the PRR in the dual domain was actually an unresolved double Mach reflection. But our results show that it is a PRR, so their conjecture is wrong. The discontinuity in the (ψ, θ) curve at θ_e is caused by the corner signal destroying the PRR and forcing the eruption of the MR ($\psi > 0$) when $\theta < \theta_e$, but being unable to do so ($\psi = 0$) when $\theta \geqslant \theta_e$.

Suppose we ignore the discontinuity and extrapolate (6.1) into the dual domain until $\psi = 0$; the extrapolation is shown as a dashed line in figure 8. Solving (6.1) with $\psi = 0$ gives $\theta = 57.006°$, and $112.29°$. The first root differs from $\theta_N = 57.021°$ by only $0.012°$. The experimental data for $\theta < \theta_e$ behave as though the discontinuity does not exist. This is plausible because ψ is an asymptotic quantity so the ramp blockage should be the dominant disturbance and not the boundary layer. Even so, only PRR has ever been observed during ramp experiments in the dual domain, so the discontinuity at θ_e must appear in the ψ experimental data as $\theta \to \theta_e$. It is difficult to measure the position of the discontinuity precisely. For by estimating with (3.1a), x_{int} increases to our ramp length (0.17 m) if θ increases from 52° to 53°, while MR is unattainable for a 53.6° ramp because $x_{int} = \infty$. Since the cavity experiments show that MR is stable in the dual domain, it is concluded that MR is suppressed on the ramp by the boundary layer. If MR could be induced by designing vigorous fluctuations into the experiments, and by modelling the fluctuations in the N-S calculations, then presumably the ψ data would lie on the dashed curve in figure 8. The self-similar MR → PRR transition should then occur at θ_N as it does in both the cavity experiments and Euler calculations. Furthermore the $x_{int} = \infty$ singularity should shift to θ_N; otherwise (5.2) is only valid for $\theta < \theta_e$.

The curve of best fit throught the N-S data (3.1b) does not agree with experiment when $\theta < \theta_e$ (table 4, figures 6, 10). This is attributed to our failure to model surface

roughness and turbulence (§5.7). The N-S equations constrain the boundary layer to be laminar, but because Re is so large, it is likely that it will be turbulent for most of its length. If modelling these items could successfully remove the x_{int} discrepancy (figure 6, table 4), then the curve of best fit throught the numerical data would agree with equation (5.2).

7. Conclusions

Shock diffraction over a ramp consists of two disturbances in the flow, namely the ramp blockage and the boundary layer on its surface.

$\theta < \theta_e$: Experiment confirms the prediction of our Navier–Stokes calculations that a precursor regular reflection appears initially on the ramp and is destroyed by an overtaking corner signal forcing the eruption of a Mach reflection. Since the PRR exists for only a limited time, it is meta-stable. A measure of where the dynamic (unsteady) PRR → MR transition takes place is the viscous length scale x_{int}, defined in the text §3.2.2, and figure 3. The length x_{int} depends on the system parameters (T_0, P_0, θ, M_i) and possibly also on the surface roughness R_a and the turbulence. It increases rapidly as $\theta \to \theta_e$ from below and or as p_0 decreases. The criterion for the dynamic PRR → MR transition is close to the e-point on the r' part of the reflected shock (figure 2b). The results show that MR is not self-similar but only asymptotically self-similar. Nevertheless with $p_0 = 14.1\,\text{kPa}$, MR becomes indistinguishable from a self-similar system over a length scale of about 0.03 m, which is much smaller than the ramp length (0.17 m).

$\theta = \theta_e$: By the N-S calculations the velocity of the corner signal becomes zero relative to the PRR node as $\theta \to \theta_e$ from below; so $x_{int} \to \infty$, as $\theta \to \theta_e$, and the PRR becomes stable.

$\theta_e \leqslant \theta \leqslant \theta_N$: Only PRR has been observed during ramp experiments in the dual domain. Consequently there is a discontinuity at θ_e in the ψ versus θ curve because there is PRR ($\psi = 0$) when $\theta > \theta_e$, and MR ($\psi > 0$) when $\theta < \theta_e$ (figure 8). Therefore the MR → RR transition is discontinuous at or near θ_e. Mach reflection has not yet been observed on a ramp in the dual domain, although it certainly has been for steady-state and self-similar reflections off planes of symmetry (§§6.1, 6.2). It is conjectured that if MR could be induced on a ramp by designing an experiment to have sufficiently large fluctuations, then presumably both the MR → RR transition and the $x_{int} \to \infty$ singularity would be shifted to θ_N.

By definition, RR has no boundary layer interaction. Examples are shock reflection off a plane of symmetry in steady-state or self-similar experiments, or in Euler calculations; RR is well described by the von Neumann theory. By contrast, PRR only appears with boundary layer interaction, as on a ramp surface. It is approximately described by the von Neumann theory for $\theta \geqslant \theta_e$, but not at all described for $\theta < \theta_e$.

REFERENCES

BARBOSA, F. J., SKEWS, B. W. & FELTHUN, L. 1997 *21st Intl Symp. on Shock Waves, Gt. Keppel Is., University of Queensland, Australia* (ed. A. F. P. Houwing). University of Queensland.

BEN-DOR, G. & GLASS, I. I. 1979 *J. Fluid Mech.* **92**, 459.

BEN-DOR, G. & GLASS, I. I. 1980 *J. Fluid Mech.* **96**, 735.

BEN-DOR, G., MAZOR, K., TAKAYAMA, K. & IGRA, O. 1987 *J. Fluid Mech.* **176**, 333.

BEN-DOR, G. 1992 *Shock Wave Reflection Phenomena.* Springer.

BLEAKNEY, W. & TAUB, A. H. 1949 *Rev. Mod. Phys.* **21**, 584.

CHPOUN, A., PASSEREL, D., LI, H. & BEN-DOR, G. 1995 *J. Fluid Mech.* **301**, 19.

COLELLA, P. & HENDERSON, L. F. 1990 *J. Fluid Mech.* **213**, 71.

COURANT, R. & FRIEDRICHS, K. O. 1948 *Supersonic Flow and Shock Waves.* Interscience.

FOMIN, V. M., HORNUNG, H. G., IVANOV, M. S., KHARITONOV, G. P. & KLEMENKOV, G. P. 1996 *The Study of Transition between Regular and Mach Reflection of Shock Waves in Different Wind Tunnels; 12th Intl Mach Reflection Symposium, University of Witwatersrand, South Africa* (ed. B. Skews).

HENDERSON, L. F. 1987 *Z. Angew. Math. Mech.* **67**, 73.

HENDERSON, L. F., CRUTCHFIELD, W. Y. & VIRGONA, R. J. 1997 *J. Fluid Mech.* **331**, 1.

HENDERSON, L. F. & GRAY, P. M. 1981 *Proc. R. Soc. Lond.* A **377**, 363.

HENDERSON, L. F. & LOZZI, A. 1975 *J. Fluid Mech.* **68**, 139.

HENDERSON, L. F. & MENIKOFF, R. 1998 *J. Fluid Mech.* **366**, 179.

HENDERSON, L. F. & SIEGENTHALER, A. 1980 *Proc. R. Soc. Lond.* A **369**, 537.

HILSENRATH, J., HOGE, H. J., BECKETT, C. W., MASI, J. F., BENEDICT, W. S., NUTTAL, R. L., FANO, L., TOULOUKIAN, Y. S. & WOOLLEY, H. W. 1960 *Tables of Thermodynamic and Transport Properties.* Pergamon.

HORNUNG, H. G. 1986 *Ann. Rev. Fluid Mech* **18**, 33.

HORNUNG, H. G. & KYCHAKOFF, G. 1977 *Proc. 11th Intl Symp. on Shock Tubes and Waves* (ed. B. Ahlborn, A. Hertzberg, A. & D. Russell), p. 296. University of Washington Press.

HORNUNG, H. G., OERTEL, H. & SANDEMAN, R. J. 1979 *J. Fluid Mech.* **90**, 541.

HORNUNG, H. G. & ROBINSON. M. L. 1982 *J. Fluid Mech.* **123**, 155.

HORNUNG, H. G. & TAYLOR, J. R. 1982 *J. Fluid Mech.* **123**, 143.

IVANOV, M. S., GIMELSCHEIN, S. F., KUDRYAVTSEV. A. N. & MARKELOV, G. N. 1996 *Numerical Analysis of Hysteresis Phenomenon in Steady Interactions of Strong Shock Waves; 12th Intl Mach Reflection Symposium, University of Witwatersrand, South Africa* (ed. B. Skews).

IVANOV, M. S., GIMELSCHEIN, S. F., KUDRYAVTSEV. A. N. & MARKELOV, G. N. 1997a *Transition from regular to Mach reflection in two-and three-dimensional flows; 21st Intl Shock Wave Symp, Gt. Keppel Is. University of Queensland, Australia* (ed. A. F. P. Houwing). University of Queensland.

IVANOV, M. S., GIMELSCHEIN, S. F., MARKELOV, G. N. & BEYLICH, A. E. 1995a *Proc. 20th Intl Symp on Shock Waves* (ed. B. Sturtevant, J. E. Shepherd & H. G. Hornung), p. 471. World Scientific.

IVANOV, M. S., GIMELSCHEIN, S. F., MARKELOV, G. N. & BEYLICH, A. E. 1995b *Phys. Fluids* **7**, 685.

IVANOV, M. S., KLEMENKOV, G. P., KUDRYAVTSEV, A. N., NIKIFOROV, S. B., PAVLOV, A. A., FOMIN, V. M., KHARITONOV, A. M., KHOTYANOVSKY, D. V. & HORNUNG, H. G. 1997b *Experimental and numerical study of the transition between regular and Mach reflections of shock waves in steady flows; 21st Intl Shock Wave Symp. Gt. Keppel Is. University of Queensland, Australia* (ed. A. F. P. Houwing). University of Queensland.

KAWAMURA, R. & SAITO, H. 1956 *J. Phys. Soc. Japan* **11**, 584.

LOCK, G. D. & DEWEY, J. M. 1989 *Exps. Fluids* **7**, 91.

MARK, H. 1958 *NACA TM* 1418.

MIRELS, H. 1956 *NACA TN* 37, p. 12.

MIRELS, H. & HAMMAN, J. 1962 *Phys. Fluids* **5**, 91.

NEUMANN, J. VON 1943 In *Collected Works*, Vol. 6. Pergamon, 1963.

PANTAZAPOL, D., BELLET, J. C. & SOUSTRE, J. 1972 *C. R. Acad. Sci. Paris* **275**, A 225.

SASOH, A. & TAKAYAMA, K. 1994 *J. Fluid Mech.* **277**, 331.

SASOH, A., TAKAYAMA, K. & SAITO, T. 1992 *Shock Waves* **2**, 277.

SKEWS, B. W. 1997 *Shock Waves* **7**, 373.

SMITH, L. G. 1945 Photographic investigations of the reflection of plane shocks in air. *OSRD Rep.* 6271.

TAKAYAMA, K. 1983 *Proc. SPIE, Indust. Applics. Laser Tech.* **398**, 174.

TAKAYAMA, K. & BEN-DOR, G. 1981 *AIAA J.* **19**, 1238.

VIRGONA, R. J. 1993 Shock wave diffraction. PhD thesis, University of Sydney, Australia.

VUILLON, J., ZEITOUN, D. & BEN-DOR, G. 1995 *J. Fluid Mech.* **301**, 37.

WALENTA, Z. A. 1983 *Arch. Mech. Warsaw* **35**, 187.

WALENTA, Z. A. 1987 *Proc. 16th Intl Symp. Shock Tubes and Waves, Aachen, Germany* (ed. H. Gronig), p. 535.

WALTON, A. J. 1992 *Three Phases of Matter*. Oxford University Press.

WHITE, F. M. 1991 *Viscous Fluid Flow*. McGraw-Hill.

WONG, H. Y. 1977 *Heat Transfer for Engineers*. Longman.